Aspect Ratio Dependence of Auger Recombination and Carrier Multiplication in PbSe Nanorods

ARTICLE *in* NANO LETTERS · JANUARY 2013

Impact Factor: 13.59 · DOI: 10.1021/nl304426y · Source: PubMed

7 AUTHORS, INCLUDING:

Richard Sandberg
Los Alamos National Laboratory
62 PUBLICATIONS **652** CITATIONS
SEE PROFILE

Wan Ki Bae
Korea Institute of Science and Technology
54 PUBLICATIONS **1,534** CITATIONS
SEE PROFILE

Weonkyu Koh
Samsung Advanced Institute of Technology
23 PUBLICATIONS **704** CITATIONS
SEE PROFILE

NANO LETTERS

Letter

pubs.acs.org/NanoLett

Aspect Ratio Dependence of Auger Recombination and Carrier Multiplication in PbSe Nanorods

Lazaro A. Padilha, John T. Stewart, Richard L. Sandberg, Wan Ki Bae, Weon-Kyu Koh, Jeffrey M. Pietryga, and Victor I. Klimov*

Center for Advanced Solar Photophysics, Chemistry Division, Los Alamos National Laboratory, Los Alamos, New Mexico 87545, United States

ABSTRACT: Nanomaterials with efficient carrier multiplication (CM), that is, generation of multiple electron−hole pairs by single photons, have been the object of intense scientific interest as potential enablers of high efficiency generation-III photovoltaics. In this work, we explore nanocrystal shape control as a means for enhancing CM. Specifically, we investigate the influence of aspect ratio (ρ) of PbSe nanorods (NRs) on both CM and the inverse of this process, Auger recombination. We observe that Auger lifetimes in NRs increase with increasing particle volume and for a fixed cross-sectional size follow a linear dependence on the NR length. For a given band gap energy, the CM efficiency in NRs shows a significant dependence on aspect ratio and exhibits a maximum at $\rho \sim 6-7$ for which the multiexciton yields are a factor of ca. 2 higher than those in quantum dots with a similar bandgap energy. To rationalize our experimental observations, we analyze the influence of dimensionality on both CM and non-CM energy-loss mechanisms and offer possible explanations for the seemingly divergent effects the transition from zero- to one-dimensional confinement has on the closely related processes of Auger recombination and CM.

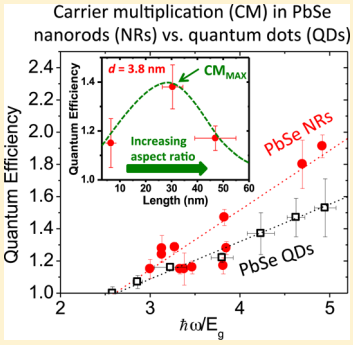

KEYWORDS: *Nanocrystal, quantum dot, nanorod, carrier multiplication, multiexciton, Auger recombination*

The desire for high-efficiency, affordable photovotaics (PVs) has motivated recent research on novel materials and photoconversion schemes that would allow one to approach and perhaps even exceed the Shockley-Queisser limit in solar energy conversion.[1,2] To this end, semiconductor nanocrystals (NCs) have emerged as a promising class of materials for practical implementation of some of the advanced PV concepts such as hot-electron extraction,[3] intermediate band solar cells,[4,5] and carrier multiplication (CM).[2,6] The first process can potentially enhance the photovoltage of solar cells, while the second can boost photocurrent. The interest in CM was greatly stimulated by the first report on spectroscopic observation of this effect in PbSe NCs,[7] which was followed by numerous experimental[8−17] and theoretical[18−26] studies of CM in NCs of various compositions. More recently, there has been a significant increase in attention to practical implementations of CM in devices such as photodetectors and PVs.[27−29]

To date, CM has been most extensively investigated for spherical semiconductor NCs, or quantum dots (QDs). Another potentially interesting class of NC materials is elongated nanoparticles, or nanorods (NRs), quasi-one-dimensional (1D) nanostructures in which enhanced carrier−carrier Coulomb interactions[30] might lead to increased CM efficiency. A further enhancement may arise from reduced symmetry in these structures, which would increase the number of multiexciton states accessible via the CM process. The use of NRs may also allow one to reduce multiexciton losses due to Auger recombination as, by elongating the particle, one can reduce the effective density of charges (and hence Auger decay rates) while simultaneously preserving a significant degree of spatial confinement, which is controlled primarily by the NR cross-sectional size.[30,31] Finally, the elongated geometry is also preferred in practical PVs as it provides a longer undisrupted pathway for photogenerated charges leading to reduced transport losses.

Recent experimental studies of CM in PbSe NRs indicated enhancement of the CM yields compared to spherical QDs.[32,33] However, the magnitude of enhancement reported in ref 32 was considerably higher than that in ref 33 for reasons that are not immediately clear. One possibility is the distortion of multiexciton dynamics due to photocharging,[34−36] which might lead to an apparent increase in the CM yields compared to "true" values.[37,38] Photocharging can be an especially serious problem in NR samples as they are known to be prone to forming a solid deposit on the walls of spectroscopic cells, which makes typical methods for mitigating photocharging, such as sample stirring, ineffective.[33] A related problem is the correct assignment of the CM component in time-resolved measurements. Species produced by CM are neutral multiexcitons (biexcitons, triexcitons, etc.), which can be identified spectroscopically on the basis of their fast decay due to Auger recombination. Auger lifetimes and their dependence on the nanoparticle volume are well documented for spherical QDs of both visible[39,40] and infrared (IR)[11,12,41] materials. However,

Received: November 30, 2012
Revised: January 21, 2013
Published: January 29, 2013

   dx.doi.org/10.1021/nl304426y | *Nano Lett.* 2013, 13, 1092−1099

there is only a limited number of studies of Auger recombination in elongated particles,[42,43] especially in the case of PbSe NRs.[43] As a result of this limited knowledge on Auger lifetimes, the difficulty in separating the Auger decay components due to charged species (produced by photocharging) and neutral multiexciton (generated via CM) could also contribute to discrepancies in the reported CM yields for NRs.

In this Letter, we present a comprehensive study of Auger recombination and CM in PbSe NRs with a range of aspect ratios and band gap energies. Our results reveal a systematic scaling of the biexciton Auger lifetime (τ_2) with NR volume (V). Specifically, for a fixed NR diameter (d), τ_2 increases linearly with increasing NR length (L). The analysis of CM efficiencies in NRs indicates a nonmonotonic dependence of the CM yield on the NR aspect ratio, ρ (defined as $\rho = L/d$), such that, independent of E_g (at least for the range of samples studied), the quantum efficiency (QE) of photon-to-exciton conversion grows with increasing ρ until it reaches a maximum at $\rho = 6-7$ and then it drops. For this optimal value of ρ, the multiexciton or CM yield (defined as $\eta = \mathrm{QE} - 1$) of the NRs exceeds that of QDs by a factor of up to ~2, consistent with the results in ref 33 but significantly lower than those in ref 32. Nevertheless, the observed enhancement is quite considerable, suggesting that shape control is a promising approach to enhance the CM efficiency of nanomaterials.

Samples and Spectroscopic Techniques. Samples investigated here are high quality, oleic-acid (OA) capped PbSe NRs grown via air-free solution-based synthesis according to the procedure reported in ref 44. In a typical reaction, 0.22 g of lead oxide (PbO) was dissolved in 5 mL of 1-octadecene in the presence of 1 mL OA. After drying under vacuum at 110 °C for 30 min, the solution was heated to 170 °C and 3 mL of a 1 M tris(diethylamino)phosphine selenide (TDPSe) solution in TDP was injected under vigorous stirring. Once the reaction finished, the reaction mixture was cooled to room temperature and mixed with hexane and precipitated by ethanol. The precipitated NRs were isolated by centrifugation and redispersed in organic solvents, typically, hexane. For spectroscopic measurements, samples were loaded into airtight cuvettes under inert atmosphere in a glovebox. Two examples of linear absorption and PL spectra for samples with mean dimensions $d = 5.0$ nm and $L = 52$ nm ($E_g = 0.63$ eV), and $d = 2.4$ nm and $L = 16$ nm ($E_g = 0.99$ eV) are shown in Figure 1, along with a transmission electron microscopy (TEM) image of the first of these two samples.

In our time-resolved spectroscopic studies, we use only samples with especially well-passivated surfaces that do not exhibit any discernible trapping component in the population decay as inferred from time-resolved spectroscopic measurements based on the absence of initial fast transients (picosecond time scales) in the regime of low-intensity, single-exciton pumping (see below); this is essential for the accurate measurements of both Auger decay times and the amplitudes of CM signals. To measure biexciton Auger lifetimes and CM yields, we monitor carrier population dynamics via either femtosecond (fs) transient absorption (TA) or transient photoluminescence (PL). In TA measurements, the excitation is either at 1.55 eV (used in studies of Auger decay and absorption cross sections) or 3.1 eV (used in CM studies). The probe pulses are derived from an optical parametric amplifier tuned to be in resonance with the band-edge $1S_h-1S_e$ transition. This experiment is performed using

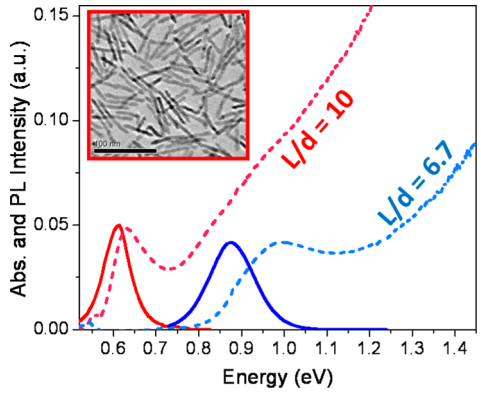

Figure 1. Absorption and PL spectra for NRs with mean aspect ratios of 10.4 and 6.7. Inset: a TEM image of the sample with $\rho = 10.4$.

100 fs (fwhm), 1 kHz pulses from an amplified Ti:sapphire laser.

In time-resolved PL measurements, the sample is excited with 1 ps pulses from a 250 kHz amplified Ti-sapphire laser. We measure transient PL signals by employing PL up-conversion (uPL) or time-correlated single photon counting (TCSPC) using excitation at 1.55 eV in the Auger recombination studies, and either 3.1 or 4.65 eV in the CM measurements. In the uPL experiment, sample emission is time-gated in a nonlinear β-barium borate crystal via frequency mixing with intense pulses of fundamental radiation at 1.55 eV.[37] The temporal resolution of this technique is defined primarily by the gate-pulse duration and is 2–3 ps in our studies. In the TCSPS measurements, sample PL is detected with a home-built cryogenically cooled superconducting nanowire single-photon detector (SNSPD)[33] coupled to photon counting electronics. The resolution in this case is limited by the width of the instrument response function (IRF) of the SNSPD system, which is ~50 ps.

We use all three techniques in both Auger decay and CM studies. Despite its lower time resolution, the SNSPD method is especially well suited for low-signal CM measurements as it has a much higher sensitivity and a lower noise level than uPL. In addition, it allows for a much faster collection of large sets of data that cover simultaneously short (tens of picoseconds) and long (microseconds) time intervals.[33] To account for a possible loss of the early time signal due to limited temporal resolution, the SNSPD traces have been corrected using a deconvolution procedure in which we utilize the experimentally measured SNSPD IRF and Auger lifetimes.[33] In the case of the NR samples studied here, the correction to the early time PL amplitude due to deconvolution is typically less than 10%.[33]

All samples were vigorously stirred during the measurements to avoid distortion of multiexciton signals due to photocharging.[37,38] For some samples, which were especially prone to forming a solid state deposit on the walls of the cuvette, in addition to stirring, we also employed slow, lateral sample translation during the measurements.[33]

Auger Recombination: Effect of Nanorod Volume. In this work, excitation levels are evaluated in terms of the average number of photons absorbed per NC per pulse: $\langle N_{ph} \rangle = j_p \sigma$, where j_p is pump fluence (number of photons per cm^2 per pulse) and σ is the absorption cross-section at the pump photon energy. To determine σ, we use the fact that below the spectroscopic threshold of CM, the average exciton multiplicity ($\langle N_x \rangle$), the average number of excitons per photoexcited NC, is

dx.doi.org/10.1021/nl304426y | Nano Lett. 2013, 13, 1092–1099

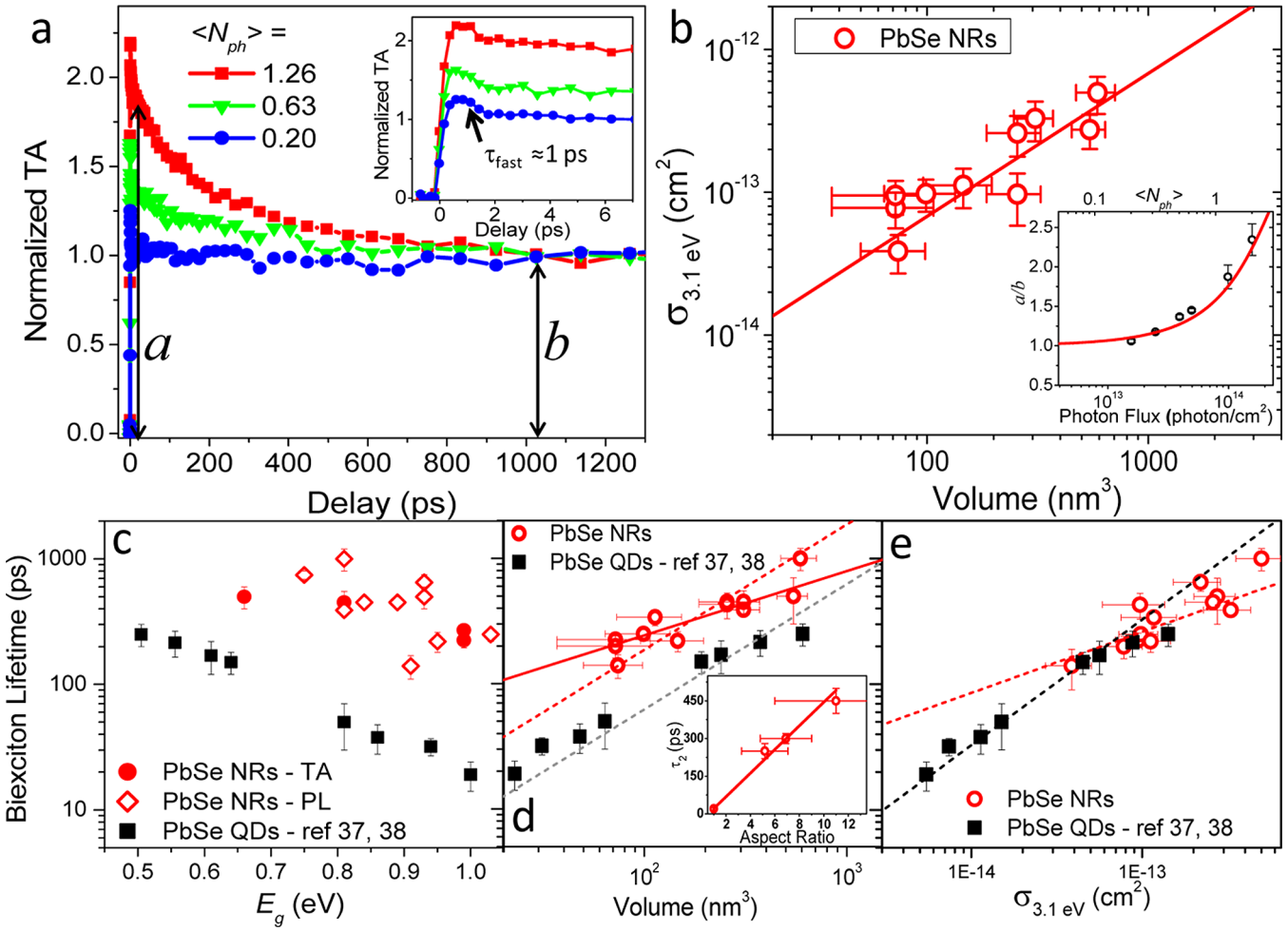

Figure 2. (a) Pump-fluence dependent TA dynamics for the PbSe NR sample with ρ = 6.7 measured using excitation at 1.55 eV; traces are normalized to unity at long times. Inset: Short-time dynamics that exhibit a fast 1 ps component likely associated with a Coulomb shift of the band-edge transition. (b) The measured 3.1 eV absorption cross sections (symbols) plotted as a function of NR volume obtained from the TEM images; line is a linear fit. Inset: The a/b ratio derived from the TA data in (a) are fitted using Poisson statistics to obtain the absorption cross-section at 1.55 eV. (c–e) Biexciton Auger lifetimes for QDs (black squares) and NRs (red solid circles and open diamonds derived from TA and PL measurements, respectively) as a function of E_g (panel c), volume (panel d), and 3.1 eV absorption cross-section (panel e). Solid line in (d) is a fit to $\tau_2 \propto (V)^{1/2}$, and dashed line is a fit to $\tau_2 \propto V$. The inset in (d) shows the dependence of τ_2 on L (symbols) for NRs with d of ca. 3.0 nm fitted to a line. Dashed red and black lines in (e) are fits to $(\sigma_{3.1eV})^m$ with m = 0.5 and 1, respectively.

governed by Poissonian statistics: $\langle N_x \rangle = \langle N_{ph} \rangle / (1 - \exp(-\langle N_{ph} \rangle))$.[45] Measuring the multiplicity (see below for the procedure) for the 1.55 eV excitation as a function of j_p and then fitting it to the Poisson dependence, we obtain the cross-section at 1.55 eV ($\sigma_{1.55eV}$). The cross-section at other photon energies can be calculated from $\sigma_{1.55eV}$ on the basis of the measured absorption spectrum.

Figure 2a shows an example of TA measurements (at 1.55 eV) that have been used to derive both $\sigma_{1.55eV}$ and the biexciton Auger lifetime (measurements in Figure 2a are for the same NR sample as one in Figure 1 with ρ = 6.7). A common feature of the recorded dynamics is a fast initial component of about 1 ps duration (inset of Figure 2a), which at low pump intensity ($\langle N_{ph} \rangle$ = 0.2) accounts for ~25% of the signal amplitude, although its relative contribution progressively decreases with increasing excitation fluence. The time scale of this early TA component is on the order of that for intraband relaxation,[46] which is typical of features due to Coulomb-interaction-induced shift of optical transitions. These features have been previously seen in TA dynamics of QDs and explained in terms of the exciton–exciton Coulumb interaction (one exciton generated by the pump pulse and the other by the probe pulse).[47,48] For the band-edge energies, this effect is especially pronounced during early stages of intraband relaxation before carriers reach the lowest energy states.[49] A fairly large amplitude of this early time signal seen in our NR samples likely results from an enhancement of Coulomb interactions associated with the quasi-1D geometry of the NRs, as discussed in ref 30.

Following the fast initial relaxation, the low-pump-intensity trace is essentially flat on the time scale of the measurements (1.3 ns), indicating the lack of any appreciable population decay due to surface trapping in these well-passivated samples. As the pump fluence is increased, we observe the emergence of a subnanosecond decay component, which is attributed to Auger decay of multiexcitons. This assignment is confirmed by analysis of the ratio of the early time signal amplitude (a; measured immediately following the initial ~1 ps spike) and the slow single-excitonic background (b). The a/b ratio derived from the TA dynamics represents a direct measure of exciton multiplicity[24,45] and, as illustrated in the inset of Figure 2b, its dependence on j_p can indeed be closely described by the Poisson dependence of $\langle N_x \rangle$. For this NR sample, the Poisson

dx.doi.org/10.1021/nl304426y | Nano Lett. 2013, 13, 1092–1099

fit yields an absorption cross-section of 1.28×10^{-14} cm^2 at 1.55 eV. From the traces for intermediate fluences ($\langle N_{ph} \rangle$ of the order of 0.5−1), we find τ_2 = 220 ps.

The measured 3.1 eV absorption cross sections of a series of NR samples are displayed in Figure 2b as a function of NR volume, V. The experimental data indicate an approximately linear scaling of $\sigma_{3.1eV}$ with V, as was previously observed for spherical QDs.[50] This scaling is a result of the bulk-like character of the QD electronic states at high spectral energies[50,51] and is applicable to all types of NCs independent of their composition or shape. At energies well above the band-edge, σ is simply proportional to the volume of a semiconductor particle and the local field correction factor f, which accounts for "incomplete penetration" of external electric field into the NC: $\sigma = \alpha_0(n_0/n_m)|f|^2V$; here, α_0 and n_0 are the absorption coefficient and the index of refraction of the semiconductor and n_m is the index of refraction of the medium surrounding the nanoparticle. From the linear fit to the experimental data in Figure 2b, we obtain $|f_{NR}|^2 \approx 0.3$. On the basis of the measurements of ref 52, the field correction factor for PbSe QDs is $|f_{QD}|^2 = 0.1$, a factor of ca. 3 smaller than for NRs. This suggests stronger field penetration into the elongated NC (i.e., reduced dielectric screening), as expected, for example, from calculations of local field corrections for nanowires versus QDs.[53]

The values of τ_2 measured for a series of NRs with various aspect ratios, using either TA (solid red circles) or transient PL (open red diamonds), are shown in Figure 2c as a function of E_g. A comparison to QDs (black squares in Figure 2c) indicates that the biexciton lifetimes in NRs are systematically longer than those in QDs with the same E_g, which is in agreement with the trend observed in ref 43. This observation is also consistent with expectations based on effective carrier density considerations. For a given E_g, elongated NRs have a greater volume than QDs[30] (spatial confinement in the NR is defined by its smaller, cross-sectional dimension), which corresponds to a lower effective carrier density, and hence, slower Auger decay.

The ambiguity in the NR volume for a given E_g leads to an apparent scatter in the τ_2 versus E_g plot in Figure 2c. In order to alleviate this ambiguity, in Figure 2d we replot τ_2 as a function of particle volume inferred from the average dimensions observed in TEM images. Immediately, we note a decrease in the apparent scatter that reveals a systematic scaling with V, that is, a monotonic increase of τ_2 with increasing NR volume. The log−log dependence of τ_2 versus V, however, is not exactly linear as in spherical QDs[39,41] (dashed black line in Figure 2d) but rather shows a spread in the slope, which varies from ∼0.5 (square root dependence; solid red line in Figure 2d) to ∼1 (linear dependence; dashed red line in Figure 2d). This spread suggests that a more rigorous description of size-dependent trends in Auger decay in NRs should account separately for changes in d and L. Indeed, the analysis of Auger lifetimes for subseries of NRs with the same cross-sectional size ($d \approx 3$ nm) but different lengths indicates that τ_2 scales linearly with L (or aspect ratio; see inset of Figure 2d). This scaling is consistent with calculations of ref 54 for bimolecular exciton−exciton annihilation in nanowires which should apply to our NR samples based on expectations that electron−hole pairs in these structures form tightly bound excitons.[30,42] The bimolecular character of Auger recombination in PbSe NRs was recently confirmed in ref 43 via the comparative analysis of the biexciton and triexciton Auger lifetimes.[55]

An inherent challenge in using the volume of the NR as the relevant parameter in the analysis of the optical observables is a large standard deviation in the NR length. Specifically, because the absorption cross-section increases with increasing particle volume, optical studies inevitably favor NRs with larger V. For this reason, we find that the use of the absorption cross-section as a proxy for the volume is more representative of the NR subensemble probed in spectroscopic studies.[50,56] In Figure 2e, we re-evaluate the dependence of the biexciton Auger lifetime on V by plotting τ_2 as a function of experimentally measured absorption cross-section at 3.1 eV. This plot suggests that τ_2 scales as $(\sigma_{3.1eV})^m$, where m varies from ∼0.5 (dashed red line in Figure 2e) to ∼1 (dashed black line in Figure 2e). As $\sigma_{3.1eV}$ is directly proportional to V (Figure 2b), this analysis confirms the validity of trends derived from direct V-dependence of τ_2 (Figure 2d). A similar analysis for the QDs (dashed black line in Figure 2d) indicates a linear proportionality between τ_2 and $\sigma_{3.1eV}$, which is in agreement with the well-known linear scaling of τ_2 with V.

One interesting observation in Figure 2e is an unexpectedly close correspondence between the τ_2 lifetimes for the NRs and the QDs for similar values of $\sigma_{3.1eV}$. This can be explained by the difference in the proportionality constants between $\sigma_{3.1eV}$ and V for dots and rods arising from the difference in the field correction factor, f, for spherical and elongated particles.[53] Specifically, our measurements of absorption cross sections of NRs presented in Figure 2b indicate that for the same volume, $\sigma_{3.1eV}$ is about 3 times larger for the NRs than for the QDs. Because of this difference, the NR data for τ_2 are shifted horizontally with respect to the QD data if plotted vs. $\sigma_{3.1eV}$, which results in the overlap of the NR and QD data points, as observed in Figure 2e. While likely coincidental, this close correspondence between NR and QD biexciton lifetimes in the τ_2 versus $\sigma_{3.1eV}$ plots is quite helpful, as it allows for the evaluation of NR Auger lifetimes on the basis of much better documented QD Auger lifetimes and readily available data for absorption cross sections.

Carrier Multiplication: Effect of Nanorod Aspect Ratio. Good quantitative understanding of Auger recombination attained from the studies of multiexciton dynamics described above is an important prerequisite for a correct assignment of CM signals and accurate quantification of CM efficiencies. QE of photon-to-exciton conversion is defined by exciton multiplicity measured in the limit of zero pump intensity (QE = $\langle N_x \rangle|_{\langle N_{ph} \rangle \to 0}$), while $\langle N_x \rangle$ can be directly inferred from TA or PL time transients recorded in the regime of low fluences when $\langle N_{ph} \rangle \ll 1$.[7,37] As was discussed earlier, due to a linear scaling of the band-edge bleach with NC excitonic occupancy, $\langle N_x \rangle$ can be directly related to the ratio of the early-to-late-time TA signal by QE = $\langle N_x \rangle = a/b|_{<Nph>\to 0}$, as amplitude b corresponds to single excitons for which $\langle N_x \rangle = 1$.[7,24] In the case of transient PL, the measured signal is proportional to the product of NC electron (N_e) and hole (N_h) occupancies ($I_{PL} \propto N_eN_h$). For neutral excitations when $N_e = N_h = N$, $I_{PL} \propto N^2$, which leads to QE = $(A/B + 2)/3|_{<Nph>\to 0}$, assuming that A/B is below 4 and hence QE is within 200%;[37,38] here, A and B are the early- and the late-time PL signals (Figure 3b).

Figure 3 shows an example of transient PL measurement with the SNSPD system[33] using excitation at 1.55 eV (a) and 3.1 eV (b) for the NR sample with $\rho = 11 \pm 5$ and $E_g = 0.89$ eV. In the low pump-fluence trace recorded with the 1.55 eV pump, we do not detect any Auger decay signatures of multiexcitons,

dx.doi.org/10.1021/nl304426y | Nano Lett. 2013, 13, 1092−1099

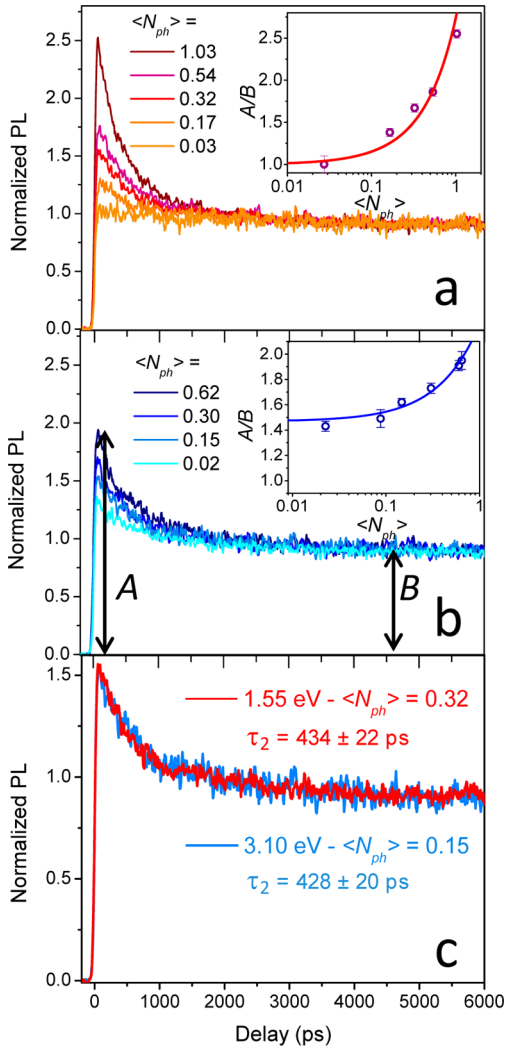

Figure 3. Pump-fluence dependent PL dynamics measured with excitation at 1.55 eV (below the CM threshold) (panel a) and at 3.10 eV (above CM threshold) (panel b). The inset in (a) shows the A/B ratio extracted from the PL traces (symbols) along with a Poissonian fit (line). The inset in (b) is the experimentally measured A/B ratios (symbols) fit to a linear dependence (line) used to extract the CM yield. (c) Comparison of PL dynamics with similar A/B ratios recorded with 1.55 and 3.10 eV excitation. The fact that these dynamics are virtually identical indicates the absence of appreciable photocharging in the CM measurements.

as expected for the situation without CM (Figure 3a). As the fluence is increased we observed the development of the biexcitonic Auger decay component, as in the previous example of TA measurements in Figure 2a. The analysis of the A/B ratio as a function of $\langle N_{ph}\rangle$ (symbols in the inset of Figure 3a) indicates that it can be described by a Poissonian dependence (line in the inset of Figure 3a), which in the case of PL signals that scale as N^2 assumes the following form: $A/B = \langle N_x\rangle(1 + \langle N_{ph}\rangle)$. The analysis of the fast component yields the biexciton Auger lifetime of 434 ± 22 ps.

In contrast to the 1.55 eV pump, the low-pump intensity limit of the A/B ratio in the case of 3.1 eV excitation is greater than unity, which is a signature of CM. In this regime, the exciton multiplicity $\langle N_x\rangle$ is non-Poissonian,[45] however, if the probability of individual CM events is independent of the number of excitons already residing in the NC, A/B can be expressed via a combination of the Poissonian probabilities and a multiexciton yield, which in the limit of low pump intensities yields $A/B = (1 + 3\eta) + \beta\langle N_{ph}\rangle$, where β is a fluence independent constant. This expression indicates that the CM yield can be derived from linear extrapolation of the measured A/B ratio to zero fluence. For the sample in Figure 3b this procedure produces $\eta = 0.16 \pm 0.04$ or QE = 1.16 ± 0.04.

To ensure that Auger decay observed at 3.1 eV indeed originates from neutral biexcitons and not from charged species (trions or charged biexcitons), in Figure 3c we directly compare the biexciton dynamics measured at 1.55 eV (red line), that is, below the spectral onset of CM ($\hbar\omega_{CM}$) to low-pump intensity PL dynamics recorded at 3.1 eV (blue line). The fact that both dynamics are identical indicates the absence of any appreciable distortion of CM measurements by photoionization, which would result in complex multiexponential Auger-decay dynamics due to contributions from both neutral and charged excitations.

The summary of CM efficiencies measured for differently sized PbSe NRs is given in Figure 4 along with the literature

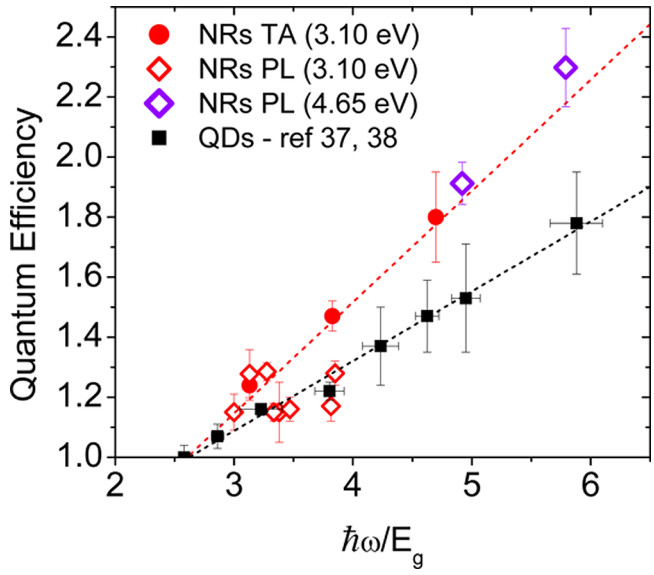

Figure 4. CM QEs measured for a series of PbSe NRs with various diameters and aspect ratios plotted as function of normalized photon energy ($\hbar\omega/E_g$); the measurements were conducted using femtosecond TA with 3.1 eV excitation (red solid circles), transient PL with 3.1 eV (red open diamonds) and 4.65 eV (purple open diamonds) excitation. The NR results are compared to literature values for PbSe QDs (black solid squares).[37,38]

results for PbSe QDs.[37,38] It is well established that CM efficiencies measured for a specific photon energy $\hbar\omega$ do not exhibit significant variations between QDs of the same E_g.[36−38] In sharp contrast, the CM yields in NRs with a similar E_g vary significantly. For example, for samples with E_g of ∼0.81 eV, QEs are from 1.17 to 1.47, which corresponds to almost a 3-fold variation in η. This indicates that the CM yields in NRs are not uniquely linked to the band gap energy.

In Figure 5, we continue our analysis of CM results by plotting CM yields as a function of NR aspect ratio spanning the range from 2 to 12. This plot exhibits less scatter in the data and suggests the existence of a systematic but nonmonotonic dependence of CM efficiency on ρ. This is also apparent in panels b−d of the same figure, where η is replotted as a

dx.doi.org/10.1021/nl304426y | Nano Lett. 2013, 13, 1092−1099

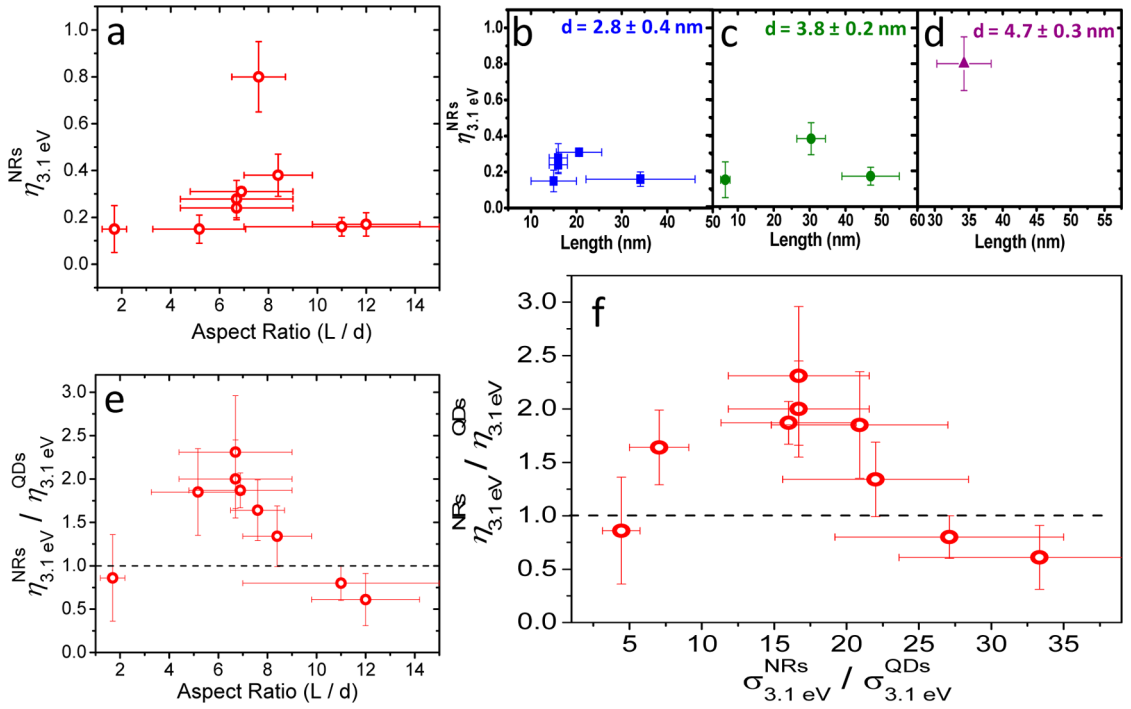

Figure 5. (a) CM yields plotted as a function of NR aspect ratio for the same series of samples as those shown in Figure 4. (b–d) The NR length dependence of the CM yield for three series of samples with diameters d = 2.8 ± 0.4 nm, d = 3.8 ± 0.2 nm, d = 4.7 ± 0.3 nm (labeled in the figure). (e) The CM yield enhancement factor for NRs versus QDs as a function of NR aspect ratio. (f) Same but using the ratio of the 3.1 eV absorption cross sections of the NRs and the QDs as a proxy for the NR aspect ratio (see text for details).

function of rod length for three subgroups of NR samples with different diameters (2.8, 3.8, and 4.7 nm). These plots indicate that two of the subgroups seem to exhibit a maximum (η_{max}) for a specific diameter-dependent value of L. Importantly, η_{max} systematically increases with increasing d, that is, reducing band gap energy, which is similar to the general trend seen for QDs (Figure 4).

In order to reveal "clean" shape-dependent trends, we remove the systematic dependence on E_g by normalizing CM yields of the NRs by those of the QDs with the same E_g. This yields the shape-dependent CM enhancement factor $\xi = \eta^{NR}/\eta^{QD}$. The plot of ξ versus aspect ratio (Figure 5e) reveals that, independent of NR diameter, ξ exhibits a well-defined maximum at ρ of 6–7. After reaching this maximum, ξ decreases with increasing ρ and for very long NRs it becomes smaller than unity, indicating not enhancement but rather a possible suppression of CM in very long NRs versus QDs.

As we saw previously in our discussion of Auger lifetimes, the scatter in the data associated with the uncertainty in the NR length can be reduced by using experimentally measured absorption cross sections as a proxy for the NC volumes. Here, we use a similar approach. Since the volume of a NR (and hence its absorption cross section) is proportional to Ld^2, while the volume of a QD with a similar E_g is proportional to d^3, the ratio of the NR to the QD absorption cross-section is proportional to L/d, that is, the NR aspect ratio. On the basis of these considerations, in Figure 5f we plot ξ as a function of $\gamma = \sigma^{NR}_{3.1eV}/\sigma^{QD}_{3.1eV}$. These data also clearly reveal the maximum in ξ and show that it occurs at $\gamma \approx 17$. This agrees with the optimum aspect ratio of 6–7, if we take into consideration that $\sigma^{NR}_{3.1eV}$ is a factor of ~3 larger than $\sigma^{QD}_{3.1eV}$ for nanoparticles of the same volume (see Figure 2b), and that for the same E_g the QD diameter is ca. 20% larger than the NR diameter.[30]

On the basis of the above results, one might suggest that the aspect-ratio dependence of QE revealed by the present study can be responsible for the discrepancy in CM yields measured for PbSe NRs in refs 32 and 33. However, our results indicate that the enhancement factor ξ is at best 2–2.3, which is in agreement with ref 33 but considerably lower than in ref 32. From the slope of the QE versus $\hbar\omega$ dependence in Figure 4, we can estimate the electron–hole pair creation energy (ε_{eh}), which is the energy required to generate a new exciton after the CM threshold is reached. If we consider only optimal samples (that is, NRs with the aspect ratio between 5 and 8, red dashed line in Figure 4), we find ε_{eh} of $2.7E_g$. By extrapolating the "optimal" linear dependence to η = 0, we determine that the CM threshold energy is ~$2.6E_g$. These values (especially ε_{eh}) represent an improvement compared to PbSe QDs, there $\hbar\omega_{CM}$ is ~$2.7E_g$ and size-average ε_{eh} is ~$4E_g$. However, they are still considerably higher than those in ref 32, where $\hbar\omega_{CM}$ and ε_{eh} (equal to ~$2.2E_g$ and ~$1.2E_g$, respectively) are near the energy conservation defined limits ($2E_g$ and E_g, respectively).

Besides the difference in aspect ratios, which can be excluded by the present study, another potential reason for very high CM efficiencies measured in ref 32 is incomplete elimination of photocharging. As discussed in ref 33, in addition to the increase in the apparent CM yield, photocharging leads to shortening of the apparent Auger time constant due to the contribution from charged biexcitons. The Auger lifetime assigned in ref 32 to neutral biexcitons is 40–50 ps, which is considerably shorter than τ_2 measured for a similar sample in the present study (~300 ps) and also in ref 43 (~150–300 ps). This again points toward a possible influence of photocharging in the measurements of ref 32.

dx.doi.org/10.1021/nl304426y | Nano Lett. 2013, 13, 1092–1099

Role of Dimensionality in Auger Decay and CM. Because of the lack of CM theory for NRs, our discussion of the effect of dimensionality will mostly rely on available experimental data and intuitive considerations. To understand the difference in CM yields between QDs and NRs, we need to consider the influence of dimensionality on both impact-ionization-like events responsible for CM (characteristic time τ_{CM}) and competing non-CM energy relaxation processes (energy loss rate k_{cool}).[11] A convenient quantity for characterizing the competition between these two energy dissipation pathways is the electron−hole pair creation energy which can be expressed as a product of τ_{CM} and k_{cool}: $\varepsilon_{eh} = k_{cool}\tau_{CM}$.[11] The value of $(\varepsilon_{eh})^{-1}$ describes the slope of the dependence of QE versus $\hbar\omega$, and higher CM efficiency implies smaller ε_{eh}. Therefore, the enhancement of CM in NRs suggests that either one or both of the quantities in the expression for ε_{eh} are reduced compared to QDs. Previous measurements of intraband relaxation in PbSe NRs[43] do not indicate any appreciable changes in the carrier cooling rate in these structures compared to the QDs, which is also in line with recent theoretical calculations suggesting that at room temperature intraband relaxation rates are similar for spherical and elongated nanocrystals.[57] This suggests that the observed enhancement in CM is likely due to shortening of τ_{CM}, implying an increased CM rate.

At first, this assessment seems to be in contradiction with the measurements of longer Auger decay lifetimes in NRs compared to QDs with the same E_g (Figure 2c). Since Auger recombination is the inverse of CM, one might expect that longer τ_2 would correspond to longer τ_{CM}. However, while this direct correspondence is indeed observed in the QDs,[11] it does not have to apply to NR samples because in this case the character of high-energy photoexcitations involved in CM is different from the character of relaxed excitations participating in Auger decay. The reason for this difference is the effect of enhanced Coulomb interactions that bind relaxed electrons and holes into tightly confined 1D excitons.[30] As a result, Auger recombination occurs not as a three-particle collision (as in QDs) but as a two-particle, bimolecular interaction between the two excitons.[42,54,58] Because of the quasi-charge-neutrality of interacting excitons, the rate of Auger decay in NRs is expected to be slower than in QDs, which is indeed observed experimentally (Figure 2c).

The role of such excitonic correlations is less significant in the case of CM, as this process involves hot unrelaxed charges before they form bound states. As a result, CM in NRs should occur in a way similar to that in QDs but with the involvement of an enhanced Coulomb interaction due to the 1D character of electronic states.[30] This enhancement is likely responsible for the increase in the CM efficiency in NRs with moderate aspect ratios (up to 6−7). The drop in the CM yields observed at larger aspect ratios is likely due to restoration of translation symmetry in the direction along the NR that imposes additional restrictions on CM due to a "turn-on" of the translation momentum conservation that may drive it back toward bulklike efficiencies. These qualitative considerations seem to consistently explain our observations for both Auger recombination and CM in NRs.

Summary. We have used a series of differently sized PbSe NR samples to analyze shape-dependent trends in Auger recombination and CM. We observe that biexciton Auger lifetimes in NRs are up to a factor 6 longer than in the QDs with the same volume and further have a linear dependence on L for NRs with a fixed cross-sectional size. The measurements of CM indicate that multiexciton yields in NRs are not a unique function of $\hbar\omega/E_g$ (as is the case in the QDs) but also exhibit a significant dependence on the aspect ratio of the particle. This dependence shows a maximum at ρ of 6−7, when the CM enhancement factor ξ reaches the value of ∼2. Increasing the aspect ratio beyond the optimal value leads to a drop in the CM yield until it becomes again comparable or perhaps even lower than in QDs. Specifically, in the longest NRs studied here (ρ of 10−12), the CM yield is ∼30−50% smaller than in the QDs with a similar E_g. To rationalize these observations, we consider the effect of dimensionality on both CM and non-CM energy relaxation mechanisms. This analysis tentatively suggests that the CM enhancement in NRs with moderate aspect ratios is primarily due to the enhancement in the Coulomb interaction associated with a 1D character of electronic states. On the other hand, the suppression of CM in longer structures may be due to restoration of translation momentum conservation, which imposes additional restrictions on the CM process. The longer Auger lifetimes in NRs in combination with enhanced CM efficiencies make them promising materials for a practical exploitation of CM in prototype generation-III PV devices.

AUTHOR INFORMATION

Corresponding Author

*E-mail: klimov@lanl.gov.

Notes

The authors declare no competing financial interest.

ACKNOWLEDGMENTS

This work was performed within the Center for Advanced Solar Photophysics (CASP), an Energy Frontier Research Center funded by the U.S. Department of Energy (DOE), Office of Science, Basic Energy Sciences (BES). We thank E. Dauler, K. Berggren, and J. Stern for providing the SNSPD devices and Martin J. Stevens, Burm Baek, and Sae Woo Nam from NIST-Boulder for help in maintaining the SNSPD.

REFERENCES

(1) Green, M. A. *Third Generation Photovoltaics: Advanced Solar Energy Consersion*; Springer: Berlin, 2003.

(2) Nozik, A. J. *Phys. E (Amsterdam, Neth.)* **2002**, *14*, 115−120.

(3) Tisdale, W. A.; Williams, K. J.; Timp, B. A.; Norris, D. J.; Aydil, E. S.; Zhu, X.-Y. *Science* **2010**, *328*, 1543−1547.

(4) Luque, A.; Martí, A. *Phys. Rev. Lett.* **1997**, *78*, 5014−5017.

(5) Luque, A.; Marti, A. *Nat. Photonics* **2011**, *5*, 137−138.

(6) Klimov, V. I. *Appl. Phys. Lett.* **2006**, *89*, 123118.

(7) Schaller, R. D.; Klimov, V. I. *Phys. Rev. Lett.* **2004**, *92*, 186601.

(8) Ellingson, R. J.; Beard, M. C.; Johnson, J. C.; Yu, P.; Micic, O. I.; Nozik, A. J.; Shabaev, A.; Efros, A. L. *Nano Lett.* **2005**, *5*, 865−871.

(9) Nair, G.; Geyer, S. M.; Chang, L.-Y.; Bawendi, M. G. *Phys. Rev. B* **2008**, *78*, 125325.

(10) Beard, M. C.; Midgett, A. G.; Hanna, M. C.; Luther, J. M.; Hughes, B. K.; Nozik, A. J. *Nano Lett.* **2010**, *10*, 3019−3027.

(11) Stewart, J. T.; Padilha, L. A.; Qazilbash, M. M.; Pietryga, J. M.; Midgett, A. G.; Luther, J. M.; Beard, M. C.; Nozik, A. J.; Klimov, V. I. *Nano Lett.* **2012**, *12*, 622−628.

(12) Beard, M. C.; Knutsen, K. P.; Yu, P.; Luther, J. M.; Song, Q.; Metzger, W. K.; Ellingson, R. J.; Nozik, A. J. *Nano Lett.* **2007**, *7*, 2506−2512.

(13) Trinh, M. T.; Polak, L.; Schins, J. M.; Houtepen, A. J.; Vaxenburg, R.; Maikov, G. I.; Grinbom, G.; Midgett, A. G.; Luther, J. M.; Beard, M. C.; Nozik, A. J.; Bonn, M.; Lifshitz, E.; Siebbeles, L. D. A. *Nano Lett.* **2011**, *11*, 1623−1629.

(14) Trinh, M. T.; Houtepen, A. J.; Schins, J. M.; Hanrath, T.; Piris, J.; Knulst, W.; Goossens, A.; Siebbeles, L. D. A. *Nano Lett.* **2008**, *8*, 1713−1718.
(15) Yang, Y.; Rodríguez-Córdoba, W.; Lian, T. *Nano Lett.* **2012**, *12*, 4235−4241.
(16) Gesuele, F.; Sfeir, M. Y.; Koh, W. K.; Murray, C. B.; Heinz, T. F.; Wong, C. W. *Nano Lett.* **2012**, *12*, 2658−2664.
(17) Miaja-Avila, L.; Tritsch, J. R.; Wolcott, A.; Chan, W. L.; Nelson, C. A.; Zhu, X. Y. *Nano Lett.* **2012**, *12*, 1588−1591.
(18) Califano, M.; Zunger, A.; Franceschetti, A. *Appl. Phys. Lett.* **2004**, *84*, 2409−2411.
(19) Allan, G.; Delerue, C. *Phys. Rev. B* **2006**, 73.
(20) Shabaev, A.; Efros, A. L.; Nozik, A. J. *Nano Lett.* **2006**, *6*, 2856−2863.
(21) Prezhdo, O. V. *Chem. Phys. Lett.* **2008**, *460*, 1−9.
(22) Rabani, E.; Baer, R. *Chem. Phys. Lett.* **2010**, *496*, 227−235.
(23) Rupasov, V. I.; Klimov, V. I. *Phys. Rev. B* **2007**, *76*, 125321.
(24) Schaller, R. D.; Agranovich, V. M.; Klimov, V. I. *Nat. Phys.* **2005**, *1*, 189−194.
(25) Luo, J. W.; Franceschetti, A.; Zunger, A. *Nano Lett.* **2008**, *8*, 3174−3181.
(26) Delerue, C.; Allan, G.; Pijpers, J. J. H.; Bonn, M. *Phys. Rev. B* **2010**, *81*, 045421 .
(27) Sukhovatkin, V.; Hinds, S.; Brzozowski, L.; Sargent, E. H. *Science* **2009**, *324*, 1542−1544.
(28) Sambur, J. B.; Novet, T.; Parkinson, B. A. *Science* **2010**, *330*, 63−66.
(29) Semonin, O. E.; Luther, J. M.; Choi, S.; Chen, H. Y.; Gao, J. B.; Nozik, A. J.; Beard, M. C. *Science* **2011**, *334*, 1530−1533.
(30) Bartnik, A. C.; Efros, A. L.; Koh, W. K.; Murray, C. B.; Wise, F. W. *Phys. Rev. B* **2010**, *82*, 195313.
(31) Li, L.-s.; Hu, J.; Yang, W.; Alivisatos, A. P. *Nano Lett.* **2001**, *1*, 349−351.
(32) Cunningham, P. D.; Boercker, J. E.; Foos, E. E.; Lumb, M. P.; Smith, A. R.; Tischler, J. G.; Melinger, J. S. *Nano Lett.* **2011**, *11*, 3476−3481.
(33) Sandberg, R. L.; Padilha, L. A.; Qazilbash, M. M.; Bae, W. K.; Schaller, R. D.; Pietryga, J. M.; Stevens, M. J.; Baek, B.; Nam, S. W.; Klimov, V. I. *ACS Nano* **2012**, *6*, 9532−9540.
(34) McGuire, J. A.; Sykora, M.; Robel, I.; Padilha, L. A.; Joo, J.; Pietryga, J. M.; Klimov, V. I. *ACS Nano* **2010**, *4*, 6087−6097.
(35) Padilha, L. A.; Robel, I.; Lee, D. C.; Nagpal, P.; Pietryga, J. M.; Klimov, V. I. *ACS Nano* **2011**, *5*, 5045−5055.
(36) Midgett, A. G.; Hillhouse, H. W.; Hughes, B. K.; Nozik, A. J.; Beard, M. C. *J. Phys. Chem. C* **2010**, *114*, 17486−17500.
(37) McGuire, J. A.; Joo, J.; Pietryga, J. M.; Schaller, R. D.; Klimov, V. I. *Acc. Chem. Res.* **2008**, *41*, 1810−1819.
(38) McGuire, J. A.; Sykora, M.; Joo, J.; Pietryga, J. M.; Klimov, V. I. *Nano Lett.* **2010**, *10*, 2049−2057.
(39) Klimov, V. I.; Mikhailovsky, A. A.; McBranch, D. W.; Leatherdale, C. A.; Bawendi, M. G. *Science* **2000**, *287*, 1011−1013.
(40) Fisher, B.; Caruge, J. M.; Zehnder, D.; Bawendi, M. *Phys. Rev. Lett.* **2005**, *94*, 087403.
(41) Robel, I.; Gresback, R.; Kortshagen, U.; Schaller, R. D.; Klimov, V. I. *Phys. Rev. Lett.* **2009**, *102*, 177404.
(42) Htoon, H.; Hollingsworth, J. A.; Dickerson, R.; Klimov, V. I. *Phys. Rev. Lett.* **2003**, *91*, 227401.
(43) Yang, J.; Hyun, B.-R.; Basile, A. J.; Wise, F. W. *ACS Nano* **2012**, *6*, 8120−8127.
(44) Koh, W.-k.; Bartnik, A. C.; Wise, F. W.; Murray, C. B. *J. Am. Chem. Soc.* **2010**, *132*, 3909−3913.
(45) Schaller, R. D.; Klimov, V. I. *Phys. Rev. Lett.* **2006**, *96*, 097402.
(46) Schaller, R. D.; Pietryga, J. M.; Goupalov, S. V.; Petruska, M. A.; Ivanov, S. A.; Klimov, V. I. *Phys. Rev. Lett.* **2005**, *95*, 196401.
(47) Klimov, V.; Hunsche, S.; Kurz, H. *Phys. Rev. B* **1994**, *50*, 8110−8113.
(48) Klimov, V. I. *Annu. Rev. Phys. Chem.* **2007**, *58*, 635−673.
(49) Klimov, V. I.; McBranch, D. W. *Phys. Rev. Lett.* **1998**, *80*, 4028−4031.
(50) Klimov, V. I. *J. Phys. Chem. B* **2000**, *104*, 6112−6123.
(51) Efros, A. L. *Semiconductors* **1982**, *16*, 772−775.
(52) Moreels, I.; Lambert, K.; De Muynck, D.; Vanhaecke, F.; Poelman, D.; Martins, J. C.; Allan, G.; Hens, Z. *Chem. Mater.* **2007**, *19*, 6101−6106.
(53) Giblin, J.; Kuno, M. *J. Phys. Chem. Lett.* **2010**, *1*, 3340−3348.
(54) Wang, F.; Wu, Y.; Hybertsen, M. S.; Heinz, T. F. *Phys. Rev. B* **2006**, *73*, 245424.
(55) Klimov, V. I.; McGuire, J. A.; Schaller, R. D.; Rupasov, V. I. *Phys. Rev. B* **2008**, *77*, 195324.
(56) Leatherdale, C. A.; Woo, W. K.; Mikulec, F. V.; Bawendi, M. G. *J. Phys. Chem. B* **2002**, *106*, 7619−7622.
(57) Chen, L.; Bao, H.; Tan, T.; Prezhdo, O. V.; Ruan, X. *J. Phys. Chem. C* **2011**, *115*, 11400−11406.
(58) Achermann, M.; Bartko, A. P.; Hollingsworth, J. A.; Klimov, V. I. *Nat. Phys.* **2006**, *2*, 557.